Construction and Building Materials 220 (2019) 464–475

Contents lists available at ScienceDirect

Construction and Building Materials

journal homepage: www.elsevier.com/locate/conbuildmat

A finite element study of rain intensity on skid resistance for permeable asphalt concrete mixes

Tianchi Tang [a,*], Kumar Anupam [a], Cor Kasbergen [a], Athanasios Scarpas [a,b], Sandra Erkens [a]

[a] *Section of Road Engineering, Faculty of Civil Engineering & Geosciences, Delft University of Technology, Stevinweg 1, 2628 CN, Delft, The Netherlands*
[b] *Department of Civil Infrastructure and Environmental Engineering, Khalifa University of Science and Technology, Abu Dhabi, P.O. Box: 127788, United Arab Emirates*

HIGHLIGHTS

- CT-scanned meshes of AC mixes representing realistic inner structures of the mix.
- FE based framework to analyze the role of various rainfall intensities on wet skid resistance.
- Parametric analysis to study the effect of various parameters on wet skid resistance-rainfall intensity relationship.
- Validation of the proposed FE model against field test data and previous empirical models.

GRAPHICAL ABSTRACT

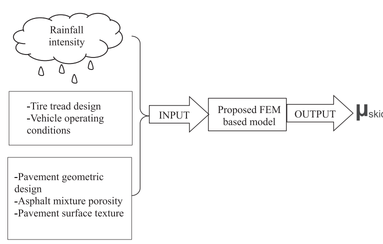

ARTICLE INFO

Article history:
Received 8 January 2019
Received in revised form 28 March 2019
Accepted 30 May 2019
Available online 24 June 2019

Keywords:
Tire-pavement interaction
Wet skid resistance
Porous pavement
Water drainage

ABSTRACT

Safe highway operations are one of the major concerns of pavement engineers and authorities. The reduction of skid resistance during rainy weather poses high risk for safe driving. Wet skid resistance varies under different rainfall intensities and is influenced by many factors such as permeability of asphalt material, pavement geometric design, and tire operating conditions. Empirical studies could offer useful understanding of mechanisms of wet skid resistance and its influencing factors, however, the applicability of the empirical relationships are restricted as soon as there is a change in one of the relevant factors. In recent years, the advancement of the finite element tools has enabled researchers to simulate the tire-fluid-pavement interaction in a more realistic way. However, to the best of the authors' knowledge, the current available numerical models either do not include the real microstructures of the pavement or ignore the water infiltration through the pavement voids in the simulations. Therefore, this paper aims to providing a numerical tool to evaluate the wet skid resistance at various rainfall intensity conditions considering the effects of pavement geometric design, tire tread design and tire operating conditions. The surface characteristics and porous microstructures of the pavement are included in the model in a way that both the vertical water flow into the asphalt concrete and surface flow on the pavement can be captured in the simulation. The effects of several pronouncing influential factors as mentioned above are quantified. Such a model upon validation is expected to provide an easy and reliable tool for pavement engineers to evaluate wet skid resistance under rainy weather more accurately which can be incorporated into pavement management systems for safety highway operation.

* Corresponding author.
E-mail address: t.tang@tudelft.nl (T. Tang).

https://doi.org/10.1016/j.conbuildmat.2019.05.185
0950-0618/

1. Introduction

Safe highway operation is of prime importance for most of the road agencies, road institutions and road organizations. According to the reports, approximately 14% of the fatal road accidents occur under wet weather conditions [1,2]. During wet weather driving conditions, the water on the pavement acts as a lubricant which reduces the contact area at the tire-pavement interface [3,4]. As a consequence, skid resistance decreases or in other words chances of skid related traffic accidents increases on wet pavements as compared to dry pavements. The adverse effect of the presence of a water film on skid resistance has been highlighted in many research studies [5,6]. In general, higher rainfall intensity results in greater water accumulation over the pavement [7,8]. Further, a combination of critical water film thickness and vehicle speed may result in significantly low skid resistance, which has been widely reported as the main cause of wet weather-related accidents [9,10]. Hence, it is necessary for road authorities and organizations to evaluate wet skid resistance at different rainfall conditions more accurately. Skid resistance at different rainfall intensities is also known to be affected by factors such as tire tread characteristics, vehicle operating conditions and pavement surface conditions which will be discussed in the following subsections.

1.1. Effect of the tire tread characteristics and vehicle operating condition

The deep-treaded tire is widely adopted as an important measure of channelling away more water at the tire-pavement contact zone [11–14]. On the other hand, worn-out tires usually cannot provide sufficient drainage capacity through their treads and hence may impact the safety of driving conditions. Therefore, legislation in many countries set a legal minimum requirement for tread depth, e.g. a minimum tread depth of 1.6 mm is specified in the UK, the US and Canada [15].

During wet weather conditions, vehicles travelling at a high speed are considered at a higher risk of skidding [6,16]. It is because there is not enough time for the water to escape the tire-pavement contact zone and hence the skid resistance reduces. In addition, tire slip ratios also affect wet skid resistance [17]. The critical slip ratio is reported to be between 7% and 25% and varies with speeds [18,19].

1.2. Effect of the pavement surface characteristics

Better surface texture affects the actual contact between the tire and pavement by facilitating the drainage of the entrapped water and hence can significantly improve wet skid resistance [20–22]. Previous studies [23,24] suggested that a deeper pavement texture is necessary to have sufficient wet skid resistance particularly for a vehicle travelling at higher speeds. Apart from the texture characteristics, the geometric design of the pavement such as the cross slope is another important factor that influences the amount of water accumulation on the pavement. Gallaway et al. [25] observed that increasing cross slope of the pavement would decrease the accumulated water depth on the pavement surface which eventually increases the skid resistance. Balmer [26] reported that both the cross slope and the macrotexture of the pavement influence water accumulation on the pavement surface during rain.

Above studies highlight that researchers have generally recommended two approaches to alleviate wet weather driving risk: a) by improving the tire drainage capability by means of proper tire tread pattern design; b) by improving drainage characteristics of the pavement surface. Although most of the road authorities make recommendations for maintaining minimum tire groove depth, research studies on optimal design characteristics such as tread pattern, tread widths etc. are mostly left to tire industries. Thus, pavement research studies focus more on improving the drainage capabilities of pavements.

Pavements with the ability to discharge surface runoff are currently recommended particularly in places where adverse weather are frequently expected [27,28]. Porous asphalt (PA) pavement which is characterized by high porosity and permeability enables rainwater to flow through the porous layers more quickly are always used in such areas. The benefits on wet skid resistance using porous asphalt pavement have been reported by various researchers [29–32].

1.3. Mechanistic-based tools to study wet skid resistance

By means of computational and analytical tools, evaluations of wet skid resistance at different rainfall conditions considering various influential factors related to tire and pavement are often far less expensive than conducting large-scale experiments. Once these models are calibrated and validated, they can predict skid resistance under different rainfall intensities with good accuracy. Mechanistic-based models will further allow getting a full theoretical vision into drainage characteristics of the asphalt mixture and tire-wet pavement interaction mechanism.

Earlier, researchers [33–36] proposed several theoretical models to study wet skid resistance where various water film depths were included to represent different rainfall conditions. However, these models were of limited use because various assumptions were made such as: water was made as inviscid and the effects of tire deformation were ignored. Later, Cho et al. [37] proposed a theoretical approach to study the rolling/skid resistance of a passenger car tire on a pavement flooded with water. The drawbacks of this model were the non-textured pavement and the ignored permeability of the pavement surface. Fwa and Ong [38,39] developed a 3D numerical model to study the effects of speed on wet skid resistance at different water depth. The transversely and longitudinally grooved pavement surfaces were included in their studies. However, the model assumed a fixed tire profile and neither the effect of the tire grooving nor the surface morphologies were considered. Zhang et al. [40] developed a finite element model to investigate the influence of the aggregate size on the porous and pavement permeability on skid resistance. However, the pore structure of the pavement was simplified as a grid network model which is not realistic and hence the percentage of the interconnected voids in the asphalt mix may not be correct. Anupam [41] proposed a tire-water-pavement interaction model to quantify the effect of the pavement texture depth on wet skid resistance. However, in this model, only a locked smooth tire was simulated which neglected the effects of different tire operating conditions such as a skidding tire with various slip ratios on skid resistance. Also, the pavement surface was artificially grooved which did not represent the real situation where the pavement surface was randomly textured. Srirangam et al. [42] and Anupam et al. [43] developed a tire-fluid-pavement interaction model to study the wet skid resistance and hydroplaning phenomena by introducing actual pavement surface morphologies. However, the drainage process of the rainwater into the asphalt mix and the effect of pavement geometric design was neglected in their models. Besides, in most of the previous studies [44–46], the accumulated rainwater depths are always determined in a separate module by using the empirical/analytical method. Such staggered methodologies, however, on one hand, simplify the complex water infiltration/flow process by considering only a set of chosen parameters; on the other hand, they neglect the fact that contact pressure at the tire-fluid interface causes changes in the fluid flow rate and hence alters the fluid flow patterns. The fluctuations in fluid flow patterns may cause a significant difference in the water depth than initially prescribed.

1.4. Objective and scope of this study

From the above literature review, it can be seen that although there have been many experimental and theoretical investigations to study the effect of different factors on the wet skid resistance, yet, limited research studies were focused on the evaluation of skid resistance under different rainfall intensities using the finite element (FE) method. It is basically due to: a) the complex interaction mechanism between tire, water and pavement structure; b) insufficient computational facilities to accurately capture the water flow path within the asphalt mixture and over the pavement surface. With the above realizations, this study proposes a FE model which can be used to evaluate the skid resistance under different rainfall intensities by accounting for the effects of the drainage characteristics of asphalt mixture, geometric design of pavement, tire tread design and various vehicle operating conditions. The proposed framework couples the simulations of water infiltration and flow process and tire-water-pavement interaction process in one module. Utilization of parallel computing techniques enables a more efficient and faster solution for the simulation. This proposed FE tool aims to provide a better and more accurate estimation of the loss of wet skid resistance associated with in-service pavement surfaces under various rainfall conditions. It is noted here that water loss due to evaporation etc. are not considered in this model.

In short, the objective of this study is to develop an innovative tire-water-pavement interaction FE model that is able to:

- evaluate the drainage characteristics of various pavement types for different rainfall conditions;
- simulate the pavement surface water flow and infiltration processes;
- quantify the effect of water discharge characteristics of a given asphalt mix design and other influential factors on wet skid resistance.
- incorporate real pavement surface textures and inner microstructures;

In order to quantify the effects of different influential factors on wet skid resistance under different rainfall intensities, the scope of the proposed study includes:

- comparison of wet skid resistance under various rainfall intensity conditions;
- comparison of wet skid resistance for different pavement cross slopes;
- comparison of wet skid resistance for different pavement mix designs;
- comparison of wet skid resistance for a given smooth tire and a given patterned tire;
- the interplay of tire-related variables such as inflation pressure, slip ratio, speed on wet skid resistance.

2. Study parameters

Two kinds of asphalt pavements were considered, namely, porous asphalt (PA) and dense asphalt concrete-10 (DAC-10). The composition and properties of each mix are shown in Table 1. Two types of tires, namely a PIARC 165R15 standard tire and a Goodyear 445/65R 22.5 truck tire, were considered in the analysis to quantify the effect of the tire tread characteristics on wet skid resistance. In this study, different vehicle operating conditions of speeds (20 km/h–120 km/h), slip ratios (10% and 100%) and pavement cross slopes (1%– 6%) are analysed. Water properties such as density were assumed at 20 °C.

3. Generation of fe meshes

3.1. Generation of pavement mesh

The details of the generation of the FE mesh of asphalt concrete pavement has been discussed in the author's previous papers [42,47]. However, for the readers' understanding, a brief description of the procedure for obtaining the FE mesh of given AC samples is provided here.

At first, the asphalt samples with a height of 60 mm and a diameter of 150 mm were cored out from the pavement test sections for both mixes (see Table 1). Subsequently an X-ray fan-beam CT scanner with a tube voltage of 225 kV was used to scan these samples at an interval of 0.4 mm in the vertical direction. Their surface morphologies and internal microstructures were captured by grayscale images with the resolution of 1430 pixels $\times$ 1430 pixels. After post-processing (i.e. filtering and segmenting) the obtained images, FE meshes for the asphalt pavements were generated by using Simpleware^{TM} software (Version 1.3; Synopsys, Inc., Mountain View, USA), as shown in Fig. 1.

3.2. Generation of tire mesh

The development of the tire model starts with the 2D FE mesh of the tire cross-section. Then, the 3D tire model was generated by revolving the 2D tire mesh about the axis representing the wheel axle.

For the development of the Goodyear truck tire, the tread and the tire body were modelled separately with different mesh densities. In this way, the computational cost for the analysis can be reduced significantly and in the meantime, the contact information at the tire-pavement interface can be retained effectively. The developed tire mesh can be seen in Fig. 2. For the purpose of calibrating the developed FE tire models, footprints obtained from a wheel load test and the numerically predicted results were compared, as can be seen in Fig. 3.

On the other hand, it is generally believed that the skid resistance of a rotating tire is mainly attributed to the hysteresis energy loss [48]. In order to quantify this energy loss, the rubber compounds are modelled as viscoelastic materials. Dynamic shear rheometer (DSR) tests are carried out to obtain the rheological

Table 1
PA and DAC-10 asphalt pavement mix compositions.

Composition					
Mixtures	4.0–10.0 mm aggregate	2.0–6.3 mm aggregate	0–4.0 mm aggregate	Limestone filler	Binder
PA	54.9%	16.8%	19.2%	3.8%	5.3%
DAC-10	17.9%	33.9%	37.7%	4.7%	5.8%
Mixtures	Density (kg/m^3)	Voids (10 gyrations)	Voids (50 gyrations)	Texture depth (mm)	Voids
PA	2582	22.7%	8.8%	1.6	23.7%
DAC-10	2387	6.3%	3.5%	0.6	3.7%

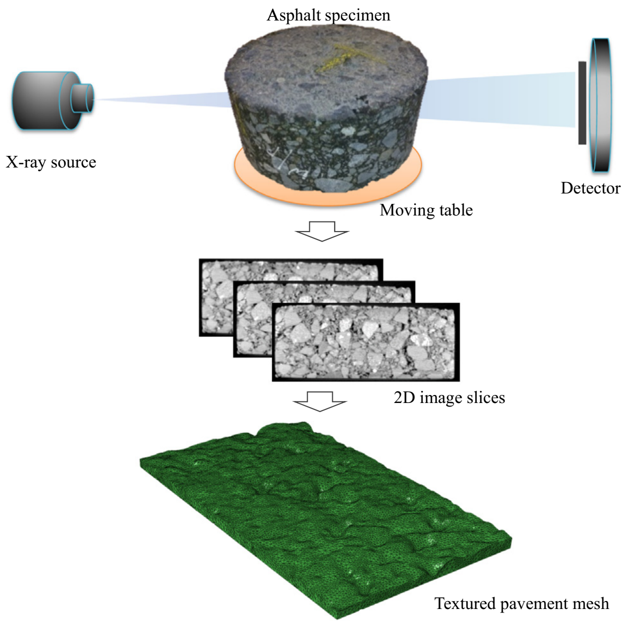

Fig. 1. Procedures for generating FE meshes of asphalt pavement surface.

parameters of the rubber compounds. For details, readers may refer to the authors' previous work [49].

4. Development of the tire-water-pavement interaction model

In the developed FE model the following interactions are considered: fluid-pavement interaction, fluid-tire interaction and tire-pavement interaction. The water is represented by the Eulerian formulation while the tire and pavement are simulated as traditional Lagrangian bodies. The coupled Eulerian and Lagrangian (CEL) technique and surface-surface contact algorithm are used to handle the interactions between the tire and pavement, tire and water, and water and pavement. The dynamic explicit analysis procedure is adopted to solve geometric and material nonlinearity.

4.1. Governing equations

The governing equations of the Lagrangian bodies (i.e. tire and pavement) are derived from the law of conservation of momentum are stated as:

$$ {}_{s}\rho D^{2}\mathbf{u}/D^{2}\mathbf{u}Dt^{2}Dt^{2} = \nabla\cdot{}_{s}\boldsymbol{\sigma} + {}_{s}\mathbf{b} \quad (1)$$

where ρ is the density, σ is the Cauchy stress, $\mathbf{b}$ is the body force. The subscript "$_s$" denotes the structure domain.

The system of fluid equations is expressed in non-conservation partial differential form as:

$$ D_{f}\rho/D_{f}\rho Dt + {}_{f}\rho\nabla\cdot\mathbf{v} = 0 \quad (2)$$

$$ {}_{f}\rho D\mathbf{v}/D\mathbf{v}Dt - \nabla\cdot{}_{f}\boldsymbol{\sigma} - {}_{f}\mathbf{b} = 0 \quad (3)$$

$$ {}_{f}\rho D\mathbf{E}/Dt - \nabla\cdot({}_{f}\boldsymbol{\sigma}\cdot\mathbf{v}) - {}_{f}\mathbf{b}\cdot\mathbf{v} = 0 \quad (4)$$

where $\mathbf{v}$ is the flow velocity and $\mathbf{E}$ is the total energy per unit volume. The subscript "$_f$" denotes the fluid domain. $\sigma\cdot\mathbf{v}$ is a function of $(p, \eta, \mathbf{v})$, where, p is pressure and η is the viscosity.

4.2. Coupling of Eulerian-Lagrangian meshes

In the CEL method, a partitioned solver is utilized to couple structure and fluid domains. The partitioned solver consists of a structure solver and a fluid solver and a coupling algorithm that couples the solvers at the interface of fluid and structure domains both in time and space. The coupling algorithm contains an interpolation method to transfer data from one domain to the other and an iteration scheme to obtain a coupled solution that is within the desired accuracy.

In Fluid-Structure-Interaction (FSI) problems fluid and structure domains are considered separately which are denoted here as ${}_{s}\partial\Omega$ and ${}_{f}\partial\Omega$ respectively. Once in contact, they share the same interface which is denoted here as $\partial\Omega^{c}$. The coupling of the fluid and the structure are governed by the following equations:

$$ {}_{s}\boldsymbol{\sigma}\cdot{}_{s}\mathbf{n} = -p_{f}\mathbf{I}\cdot{}_{f}\mathbf{n} + {}_{f}\boldsymbol{\sigma}\cdot{}_{f}\mathbf{n} \quad (5)$$

$$ {}_{s}\mathbf{u} = {}_{f}\mathbf{u} \quad (6)$$

where, ${}_{s}\boldsymbol{\sigma}$ and ${}_{f}\sigma$ denote stress tensor for the structure and viscous stress tensor for the fluid, p is the pressure field of the fluid, ${}_{s}\mathbf{n}$ is the normal of the interface at the structure side, ${}_{f}\mathbf{n}$ is the normal of the interface at the fluid side, $\mathbf{I}$ is the Identity tensor, ${}_{f}\mathbf{u}$ is the displacement tensor of the fluid, and ${}_{s}\mathbf{u}$ is the displacement tensor of the structure.

Eq. (5) indicates that the tractions on both fluid and structure sides are in balance. Similarly, Eq. (6) applies the compatibility condition between the fluid-structural displacements at the interface.

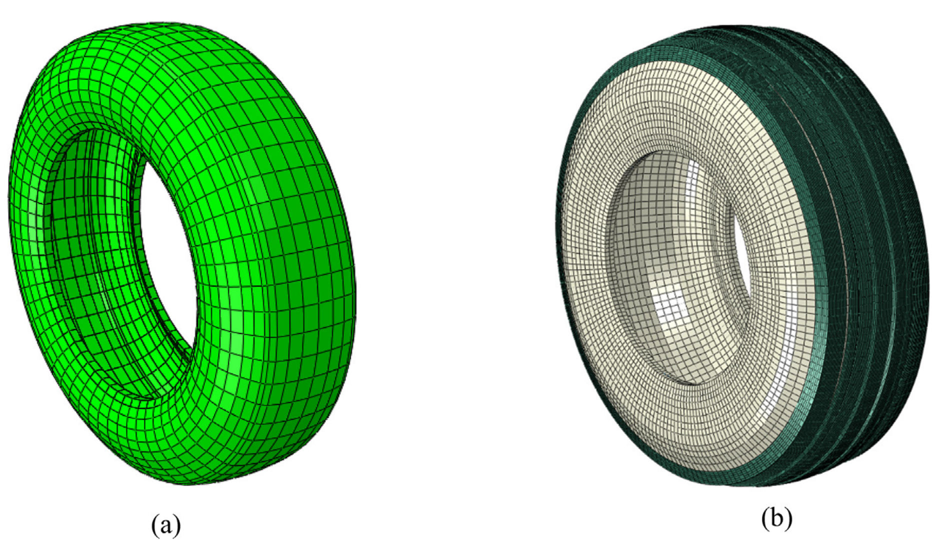

Fig. 2. Tire FE mesh: (a) smooth tire mesh; (b) grooved truck tire mesh.

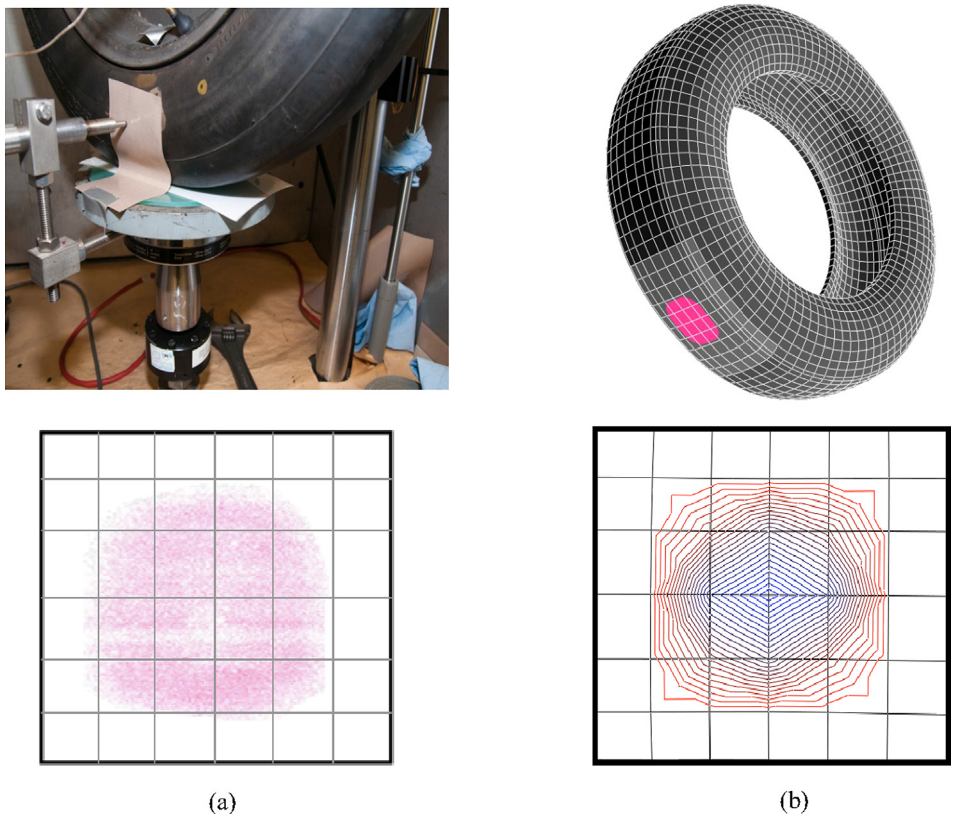

Fig. 3. Comparison of footprints at the load of 2 kN and the inflation pressure of 200 kP: (a) experiment result (b) FE modelling result.

Generally, the fluid and structure domains have different mesh refining requirements. In the case of non-matching mesh densities, the coupling of the displacement field of the two domains at the contact interface can be realized by:

a) projecting each fluid grid node S_j to the closest point S_i on the structural element ${}_{s}\Omega_{e} \in {}_{s}\partial\Omega$, where ${}_{e}$ denotes element.
b) determining the coordinates χ_j of the projected node S_i on ${}_{s}\Omega_{e}$.
c) interpolating ${}_{f}u$ inside ${}_{s}\Omega_{e}$ to obtain:

$$ {}_{f}u_{j} = {}_{f}u(S_j) = {}_{s}u\left(\chi_j\right) = \sum_{i=1}^{i=i_e} N_i\left(\chi_j\right){}_{s}u_i \quad j \in {}_{f}\partial\Omega,\ i \in {}_{s}\partial\Omega \tag{7} $$

Apart from matching the displacement fields, the laws of conservation of energy also needs to be satisfied. The virtual work due to traction acting on ${}_{f}\partial\Omega$ can be written as:

$$ \begin{aligned} {}_{f}\delta W &= \int_{{}_{f}\partial\Omega} (-p_f\mathbf{n} + {}_{f}\boldsymbol{\sigma}\cdot{}_{f}\mathbf{n})\,{}_{f}u\ ds \\ &= \sum_{j=1}^{j_f}\int_{{}_{f}\partial\Omega}(-p_f\mathbf{n} + {}_{f}\boldsymbol{\sigma}\cdot{}_{f}\mathbf{n})D_{jf}u_j\ ds = \sum_{j=1}^{j=j_f}\Phi_{jf}u_j \end{aligned} \tag{8} $$

where D_j is an extrapolation function on ${}_{f}\partial\Omega$ and Φ_j is defined as the numerical flux.

Eq. (9) describes the relation in the discretized form which can be obtained by Eqs. (7) and (8),

$$ \begin{aligned} {}_{f}\delta W &= \sum_{i=1}^{i=i_S}\left(\sum_{j=1}^{j=j_f} N_i\left(\chi_j\right)\left(-p\left(\chi_j\right)n + {}_{f}\sigma\left(\chi_j\right)\cdot{}_{f}n\right)\right){}_{s}u_i \\ &= \sum_{i=1}^{i=i_S}\left(\sum_{j=1}^{j=j_f}\Phi_j N_i\left(\chi_j\right)\right){}_{s}u_i \end{aligned} \tag{9} $$

On the other hand, the virtual work due to the structural forces on ${}_{s}\partial\Omega$ can be represented as

$$ {}_{s}\delta W = \sum_{i=1}^{i=i_S} f_i\,{}_{s}u_i \tag{10} $$

Since the energy is conserved at the interface, Equation (11) can be obtained by comparing Eqs. (10) and (11):

$$ f_i = \sum_{j=1}^{j=j_f}\Phi_j N_i(\chi_j) \tag{11} $$

The shape functions in finite element must satisfy $\sum_{i=1}^{i=i_e} N_i = 1$ and thus the nodal loads in Equation (11) should fulfil the condition shown in Eq. (12)

$$ \sum_{i=1}^{i=i_S} f_i = \sum_{i=1}^{i=i_S}\sum_{j=1}^{j=j_f}\Phi_j N_i(\chi_j) = \sum_{j=1}^{j=j_f}\Phi_j \tag{12} $$

4.3. Computation of wet skid resistance

In this model, the theory of hysteresis energy loss is used to calculate the skid resistance. A detailed description of the calculation procedure could be found elsewhere [47]. A brief description of the procedure is presented below.

The viscous work can be expressed by the following evolution equation:

$$ {}^{t+\Delta t}W_V = {}^{t}W_V + (S_e : L_v)\cdot\Delta t, \quad {}^{0}W_V = 0 \tag{13} $$

where S_e is the elastic second Piola-Kirchhoff tensor and L_v is viscous spatial velocity gradient tensor.

The energy loss ΔW per element per time step can be written as:

$$\Delta W = \int_0^{\Delta T} S_e : L_v dt \tag{14}$$

The total energy loss over the time for one tire revolution can be obtained as:

$$\Delta W = \sum_{m=1}^{M} \sum_{k=1}^{K} \int_0^T S_e^{km} : L_v^{km} dt \tag{15}$$

where $k = 1, 2, \ldots, K$ is the number of partitions in the tire model and $m = 1, 2, \ldots, M$ is the number of elements in each partition.

4.4. Boundary conditions of water inflow and outflow

The top inlet was prescribed with a velocity boundary condition to control the rainfall intensity at a distance of 150 mm above the pavement surface. The side boundaries were modelled as a zero-pressure outlet (i.e. atmospheric pressure) [41] to allow the water to flow freely out of the pavement surface. After the water passes the pavement surface layer, its flow rate will be controlled by the permeability of the pavement sub-layers (base, subbase and subgrade). Therefore, according to the previous experimental studies [50], the bottom of the pavement was prescribed with an outlet velocity of 8 mm/hr. In addition, body force was applied to the Eulerian region as shown in Fig. 5.

4.5. Analysis framework to evaluate the wet skid resistance

As mentioned earlier, the current framework couples the simulations of water flow/infiltration process and tire-water-pavement interaction process. The overall framework (as shown in Fig. 4) is as follows:

- As the first step, a steady state analysis was carried out. In this analysis a 3D tire is translated horizontal and rotated along the axle considering a smooth plane pavement. Tire contact patch (footprint) was obtained and verified with the experimental data within 1% accuracy. The deformations, stresses and strains state variables of tire mesh are stored for subsequent analysis.
- In the second step, the water body is allowed to flow sideways and vertically under the influence of gravitational force. Since, the bottom outflow condition (see Fig. 5) depends upon the capability of pavement course underneath to drain out water, then, if inflow becomes greater than this outflow, water accumulation on the pavement surface is bound to happen. It is noted here that the bottom outflow is one of the boundary conditions in the model. Once a steady state flow is reached, a constant water film thickness will be obtained as the distance between the top of the pavement surface and the top of the fluid surface. The next step of the simulation is carried out considering this condition as an initial condition.
- As the third step, analysis of the tire-water-pavement interaction was carried out to compute wet skid resistance (see Fig. 6). The tire mesh, as developed in the first step, was allowed to move with prescribed operating conditions such as axle load, tire inflation pressure, speed and slip ratio on the wetted pavement. Fig. 7 shows the comparison of the tire-water-pavement contact footprint when water film is thick and that when water film is thin for PA pavement under the same tire operating conditions. Wet skid resistance was finally computed using the procedures developed in the previous section.
- Step 1 to Step 3 are repeated with different input parameters to carry out a sensitivity analysis.

5. Model validation

The proposed FE model is validated in term of two aspects: the water depth prediction and the skid resistance prediction.

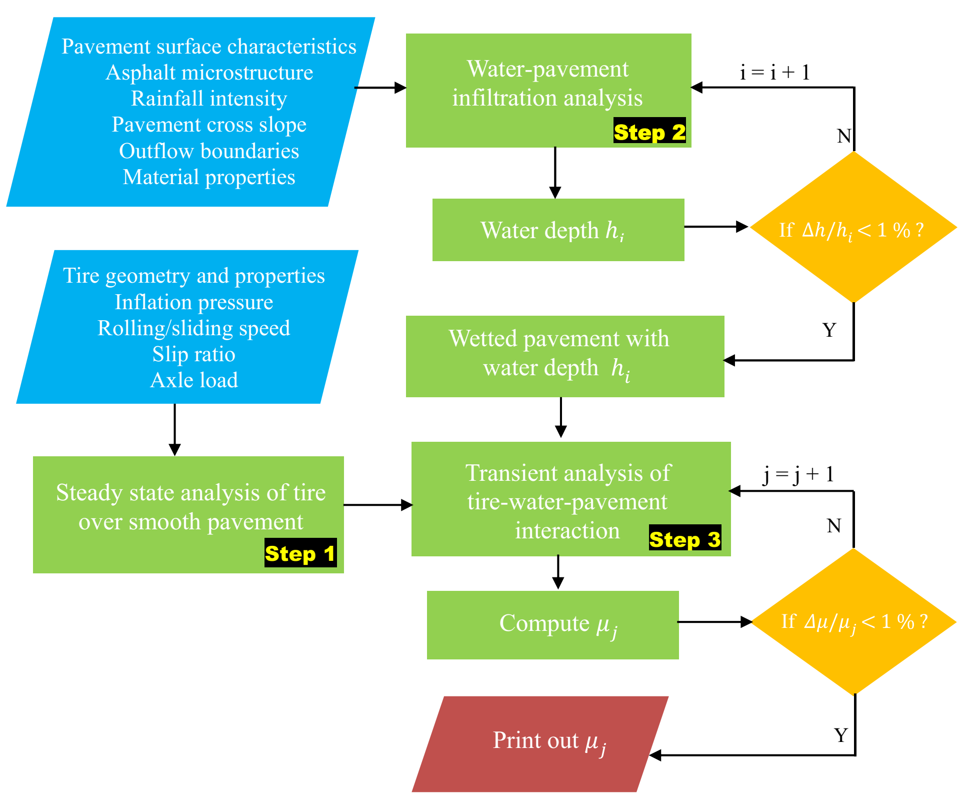

Fig. 4. Framework of determination of wet skid resistance.

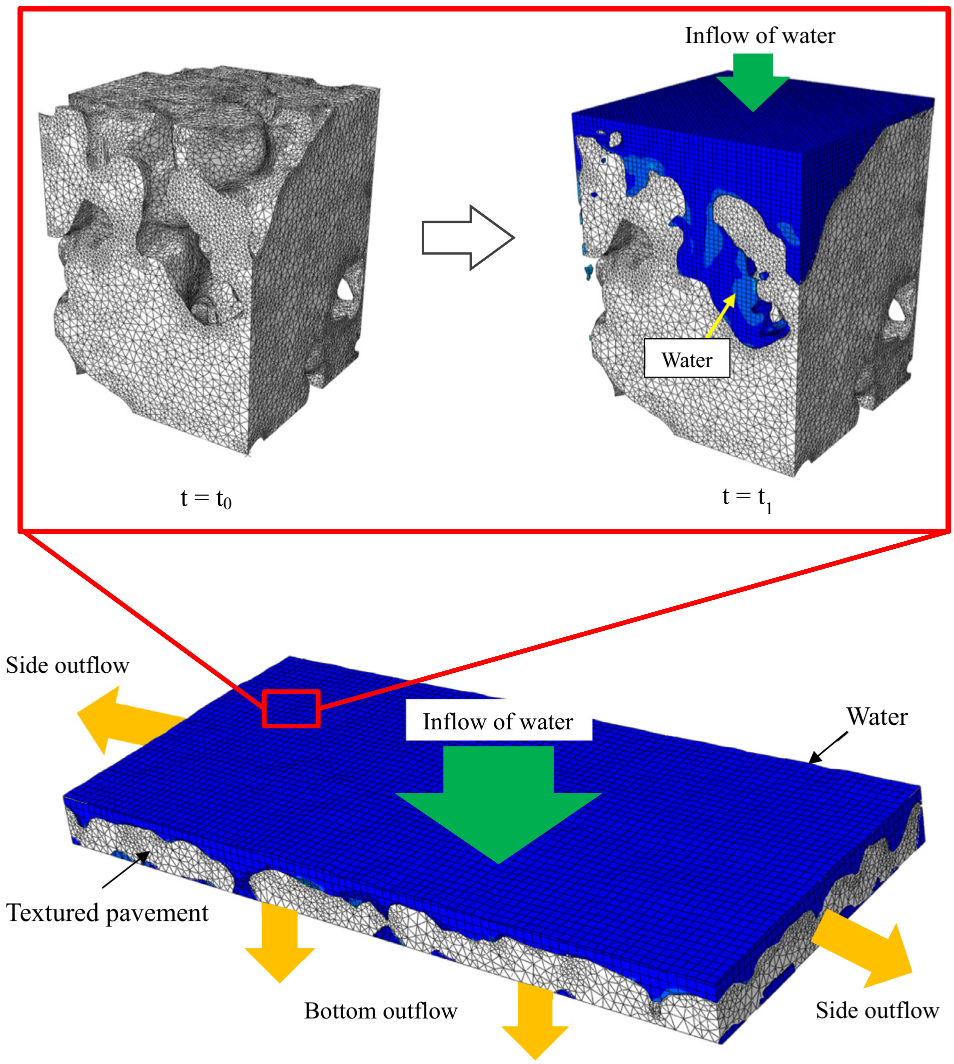

Fig. 5. Simulation of the water infiltration process.

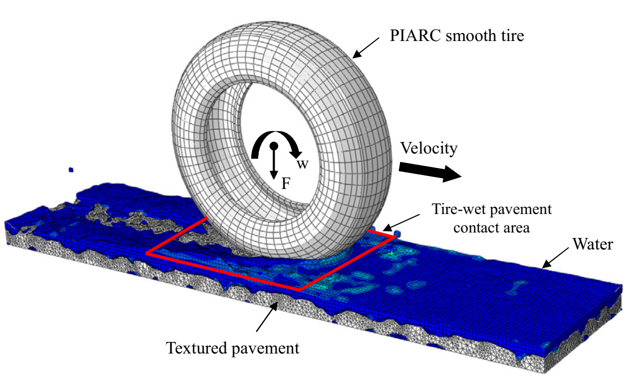

Fig. 6. Tire-water-pavement interaction process.

5.1. Model validation in terms of skid resistance prediction

The validation of the developed FE model for wet skid resistance prediction was carried out by comparing with the field measurements, as shown in Fig. 8. The parameters investigated in the field tests can been seen in Table 2.

The detailed description of the test equipment and process can be found elsewhere [42]. Fig. 9 and Table 3 compare the experiment and simulation results of wet skid resistance for a passenger car tire on a porous asphalt surface operating at four different speeds (40, 60, 90, and 120 km/h), two slip ratios (10% and 100%), and two different water film thicknesses (2.5 mm and 5 mm). The comparison results show a good agreement between simulations and field tests, allowing for the unavoidable differences in field conditions and accuracy of the instrument.

5.2. Model validation in terms of water depth prediction

The predicted water depth by the FE simulation was compared against the water depth calculated from empirical models developed by Gallaway et al [25] and Transport Research Laboratory (TRL,UK) [51]. As shown in Fig. 10, the predicted water depths are within a reasonable range considering variances in the environmental factors and test conditions under which those empirical models are developed.

6. Results and discussion

In this section, different input parameters related to the rain, pavement, and tire are investigated to quantify the effects of their variations on wet skid resistance. The results are discussed in each of the subsections.

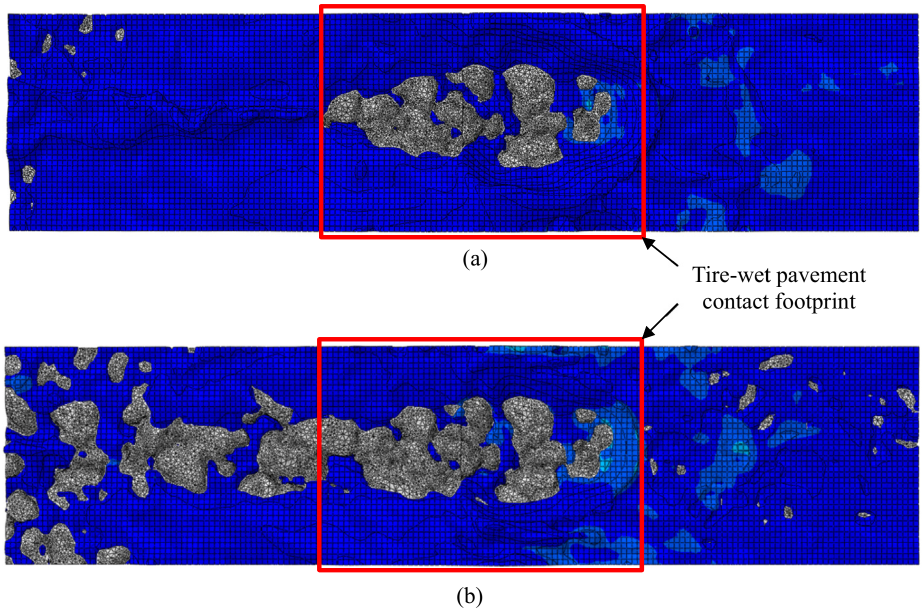

Fig. 7. Comparison of the tire-water-pavement contact footprint under same tire operating conditions: (a) with thick water film and (b) with thin water film.

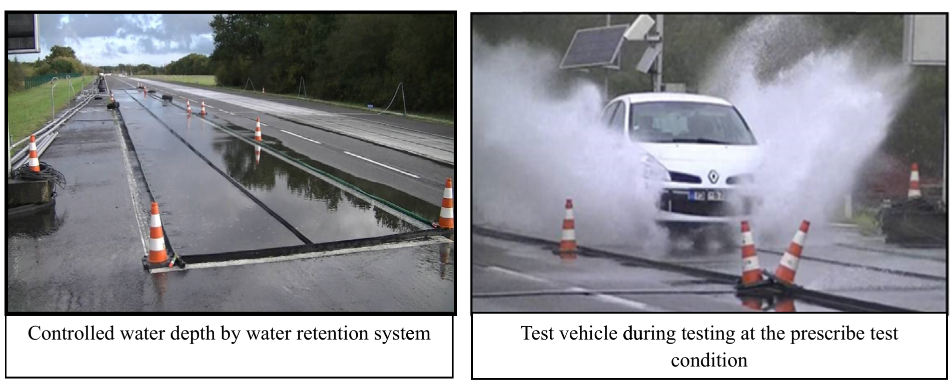

Fig. 8. Field testing of wet skid resistance (after [42]).

Table 2
Parameters for field tests.

Pavement types	Water thickness (mm)	Slip ratio (%)	Velocity (km/h)	Inflation Pressure (kPa)	Load (kN)
PA 0/6 and DAC 0/10	2.5/5	10/100	40, 60, 90 and 120	220	4.29

6.1. Influence of rainfall intensity on skid resistance

Fig. 11 shows the variations of skid resistance with rainfall intensity for DAC pavement and PA pavement under various speeds. With other parameters kept the same, skid resistance decreases with increasing rainfall intensity for both pavements, which is consistent with previous studies [5,6]. Generally, under the same rainfall condition, PA pavement offers higher wet skid resistance than the DAC pavement. For example, at a speed of the 120 km/h, the increase of the rainfall intensity from 50 to 100 mm/hr decreases the skid resistance on the PA pavement by 5% (from 0.73 to 0.69) while that on DAC pavement is 11% (from 0.52 to 0.46). It can also be found that at high rainfall intensity, the decreasing rate of the skid resistance on PA pavement is lower than that on DAC pavement. This indicates that under extreme conditions (high speed and high rainfall intensity), DAC pavement is more susceptible to insufficient skid resistance induced accidents than PA pavement.

6.2. Influence of cross slope on wet skid resistance

Fig. 12 shows the effects of pavement cross slope on wet skid resistance under various speeds. The rainfall intensity is set at 100 mm/h for all cases. It can be seen that the skid resistance increases with increasing cross slope for both pavement types. This effect is more pronounced for the PA pavement than the DAC pavement. For example, at the speed of 120 km/h, the increase of the cross slope from 1% to 6% results in the increase of skid resistance on the PA pavement from 0.69 to 0.76 (10%) whereas that increase on DAC pavement is from 0.5 to 0.52 (4%). It is also highlighted that the largest increase in skid resistance is from cross slope 1% to 3% (75% of the total increase for PA pavement, 60% of the total increase

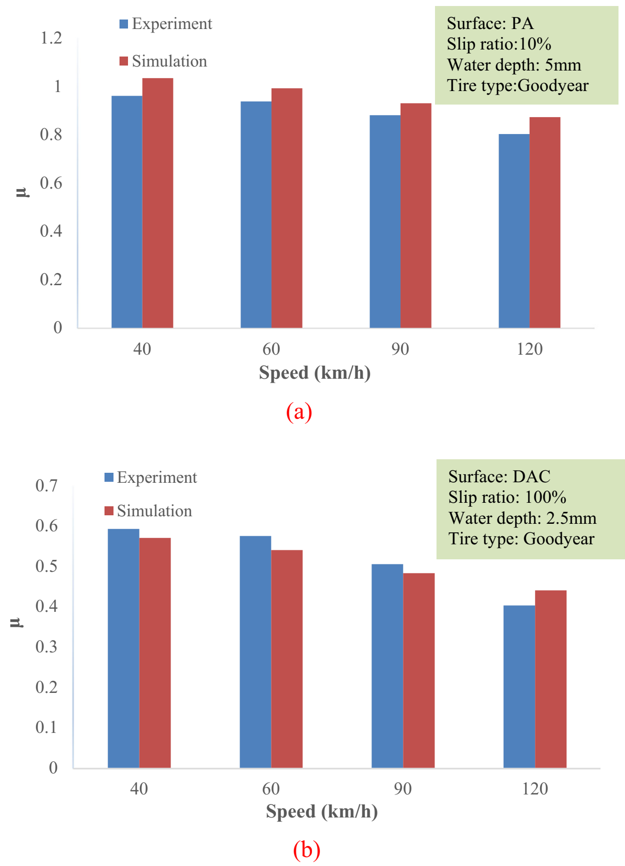

Fig. 9. Comparison of the skid resistance with experimental data.

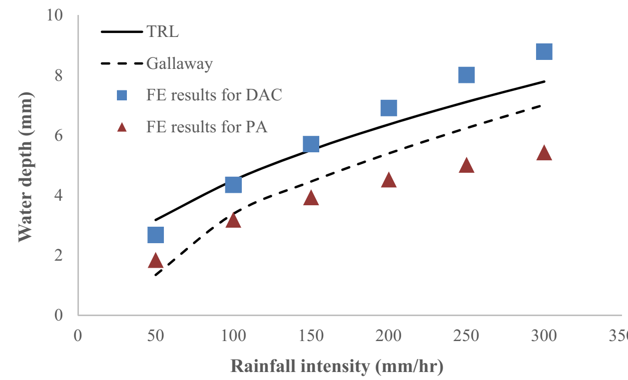

Fig. 10. Comparison of the water depth with previous empirical models.

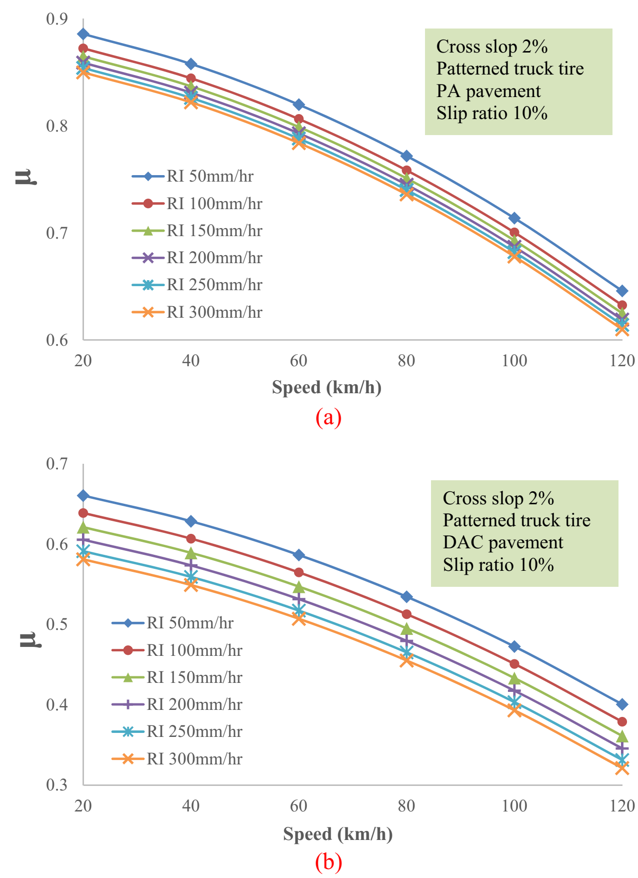

Fig. 11. Schematic of the effect of rainfall intensity (RI) on skid resistance: (a) PA pavement; (b) DAC pavement.

for DAC pavement). This implies that the drop in skid resistance beyond the cross slope 3% is marginal from the practical point of view and thus the cross slope 3% is recommended in terms of optimal pavement drainage design.

6.3. Influence of MPD on wet skid resistance

To evaluate the effect of MPD on wet skid resistance, two types of asphalt mixture, as mentioned previously, PA and DAC are utilized for simulations. The MPD of the PA is 1.6 mm while that of DAC is 0.6 mm. As shown in Fig. 13, a pavement with higher MPD offers higher wet skid resistance. For this case, at the speed of 120 km/h, the increase of MPD by 1 mm leads to an increase of skid resistance from 0.53 to 0.72 (36%). It shows the need of maintaining adequate pavement roughness to combat against skid related accident during wet weather as confirmed by previous research studies [12,21,29]. Such information could be easily embedded in pavement management databases for the road

Table 3
Errors between results from experiments and simulations.

	Speed (km/h)	40	60	90	120
PA	Experiment	0.96	0.94	0.88	0.8
	Simulation	1.03	0.99	0.93	0.87
	Error	+0.07	+0.05	+0.05	+0.07
DAC	Experiment	0.59	0.57	0.5	0.4
	Simulation	0.57	0.54	0.48	0.44
	Error	−0.02	−0.03	−0.02	+0.04

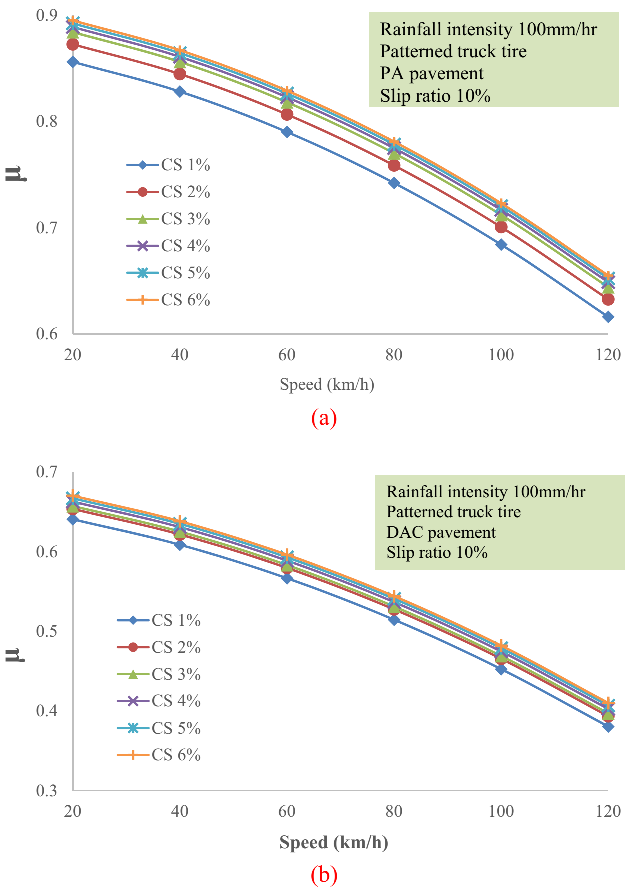

Fig. 12. Schematic of the effect of cross slope (CS) on skid resistance: (a) PA pavement; (b) DAC pavement.

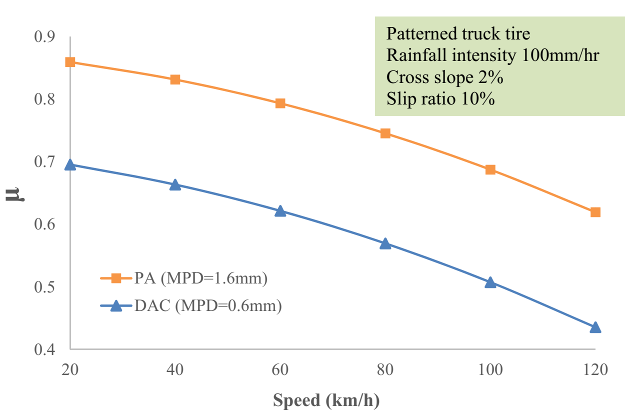

Fig. 13. Comparison of wet skid resistance on PA and DAC at different speeds.

authorities to come up with optimal planning and scheduling of road maintenance schemes.

6.4. Influence of tire tread on wet skid resistance

In order to study the effect of the tire tread pattern on wet skid resistance, two types of tires namely a PIARC smooth tire and a grooves truck tire were simulated. Fig. 14 shows that at all speeds, the patterned tire offers higher wet skid resistance than the smooth tire for both of the given pavements. The critical condition is when the smooth tire travels on a DAC pavement at the highest speed. The corresponding skid resistance coefficient of 0.08 makes

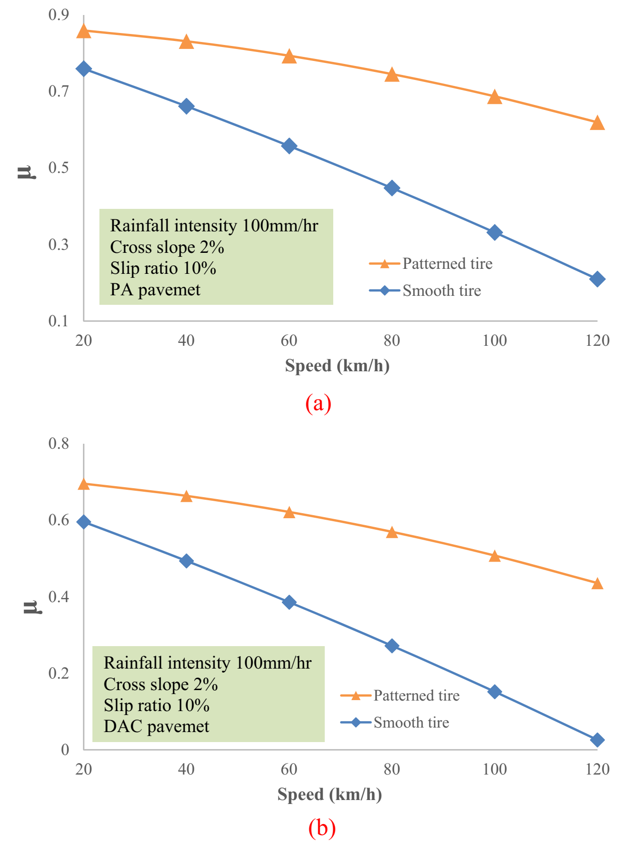

Fig. 14. Schematic of the effect of tire tread on skid resistance: (a) PA pavement; (b) DAC pavement.

the vehicle highly prone to losing directional control. It can also be seen that on the same pavement surface, with increasing speed, that the rate of decreasing skid resistance for the smooth tire is higher than that of the patterned tire.

6.5. Influence of slip ratio on skid resistance

The proposed model is capable of evaluating the effect of slip ratio on wet skid resistance. Fig. 15 shows that wet skid resistance decreases while the slip ratio increase from 10% to 100%. The rate of decrease in wet skid resistance is more noticeable for fully locked tire (100% slip) than an anti-locked wheel during a braking operation on both pavement surfaces. Lower wet skid resistance was observed for a fully locked tire denoting that there is a higher risk for accidents. With increasing speed, the average percentage decrease in wet skid resistance for a 10% slip tire is 34% for the PA pavement and 59% for the DAC pavement. The results show the effectiveness of an anti-lock braking system in enhancing safety driving.

7. Summary of results

For the ease of the readers' understanding, a summary of all the results is presented in Table 4. This table shows the relationship between μ against friction-speed gradient (G) (the definition of G can be found in [52]), improvement in cross slope (CS) and an increase in rainfall intensity (RI) on an average basis. On the basis of the results, the following conclusions can be drawn:

- irrespective of pavement type, G40-G120 is higher than G40-G80, which means the higher the speed the lesser is μ;

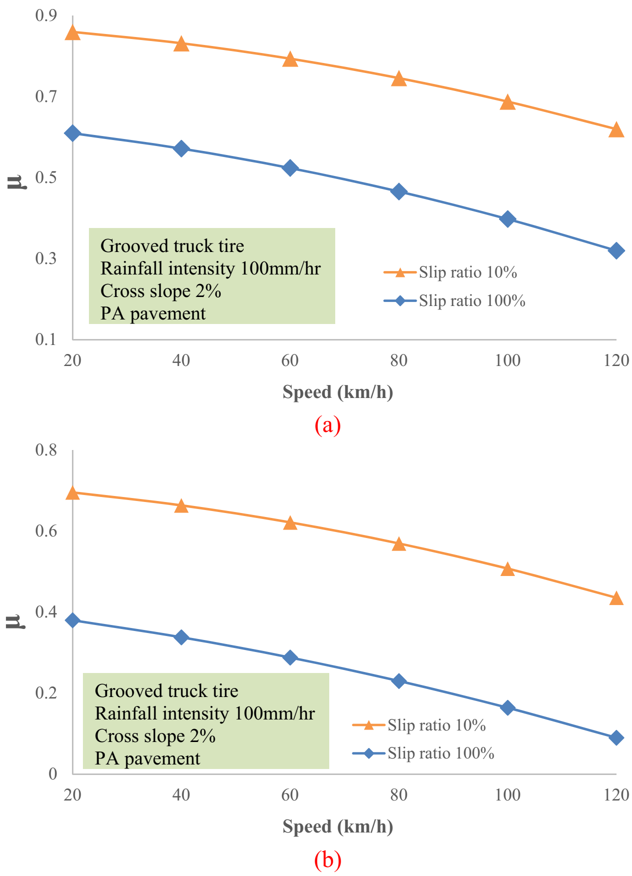

Fig. 15. Schematic of the effect of slip ratio on skid resistance: (a) PA pavement; (b) DAC pavement.

- improving cross slope decreases μ for both surface types, which indicates higher cross slopes provides better safety against skidding;
- Increase in rain intensity decreases μ. This highlights that considering a better estimation of rain intensities while designing pavement is a good practice;
- PA surfaces not only demonstrate higher skid resistance values than DAC but they also seem to be slightly more resilient to the adverse change in conditions (increasing rainfall intensity and increasing speed).

8. Conclusions

This paper presents an innovative tire-water-pavement interaction FE model with the aim to evaluate wet skid resistance under different rainfall intensities considering the effects of pavement geometric design, tire tread design and various tire operating conditions. As opposed to some widely used FE models, the proposed FE model incorporates the real pavement surface textures and inner microstructures of the AC mixes into the pavement mesh by means of CT scanning. Hence, the proposed FE model is not only able to simulate water flowing on the pavement surface but also capture the process of water infiltrating into the porous structure of the pavement. Thus, the tire-water-pavement interaction process is simulated more realistically and wet skid resistance results are obtained more accurately. The proposed FE model was validated against the results from the previous empirical models and field data.

The capabilities of the FE model were illustrated by quantifying the effects of various parameters on wet skid resistance as mentioned above. It was highlighted that the risk of safe driving conditions significantly increases for a vehicle travelling at high speed under high rainfall intensities. It is also recommended that a pavement with higher porosity and MPD values and a passenger/truck tire with a proper tread pattern are necessary for the increment of wet skid resistance and hence improves the safety driving conditions. Such an FE tool with its capability to directly link rainfall intensity and wet skid resistance for an in-service pavement could, therefore, help pavement authorities to come up with effective engineering measures to ensure safer driving conditions especially during rainy weather.

Table 4
Summary of results.

Pavement type	Change in condition	Change in μ
PA	Friction-speed gradient (20 km/h-40 km/h)	−0.028
	Friction-speed gradient (20 km/h-60 km/h)	−0.066
	Friction-speed gradient (20 km/h-80 km/h)	−0.114
	Friction-speed gradient (20 km/h-100 km/h)	−0.172
	Friction-speed gradient (20 km/h-120 km/h)	−0.24
	Improving cross slope from 1% to 2%	+0.017
	Improving cross slope from 1% to 3%	+0.028
	Improving cross slope from 1% to 4%	+0.033
	Improving cross slope from 1% to 5%	+0.036
	Improving cross slope from 1% to 6%	+0.039
	Increase in rain intensity from 50 mm/h to 100 mm/h	−0.013
	Increase in rain intensity from 50 mm/h to 150 mm/h	−0.02
	Increase in rain intensity from 50 mm/h to 200 mm/h	−0.027
	Increase in rain intensity from 50 mm/h to 250 mm/h	−0.032
	Increase in rain intensity from 50 mm/h to 300 mm/h	−0.036
DAC	Friction-speed gradient (20 km/h-40 km/h)	−0.032
	Friction-speed gradient (20 km/h-60 km/h)	−0.074
	Friction-speed gradient (20 km/h-80 km/h)	−0.126
	Friction-speed gradient (20 km/h-100 km/h)	−0.188
	Friction-speed gradient (20 km/h-120 km/h)	−0.26
	Improving cross slope from 1% to 2%	+0.013
	Improving cross slope from 1% to 3%	+0.017
	Improving cross slope from 1% to 4%	+0.022
	Improving cross slope from 1% to 5%	+0.026
	Improving cross slope from 1% to 6%	+0.029
	Increase in rain intensity from 50 mm/h to 100 mm/h	−0.022
	Increase in rain intensity from 50 mm/h to 150 mm/h	−0.039
	Increase in rain intensity from 50 mm/h to 200 mm/h	−0.055
	Increase in rain intensity from 50 mm/h to 250 mm/h	−0.069
	Increase in rain intensity from 50 mm/h to 300 mm/h	−0.079

– decrease in skid resistance; + increase in skid resistance.

Declaration of Competing Interest

None.

References

[1] T. Chelliah, P. Stephanos, T. Smith, B. Kochen, Developing a design policy to improve pavement surface characteristics, Pavement Evaluation Conference, 2002, Roanoke, Virginia, USA, 2002.
[2] D. Kuemmel, R. Sontag, J. Crovetti, A. Becker, J. Jaeckel, A. Satanovsky, Noise and Texture on PCC Pavements. Final report multi state study, Report Number WI/SPR-08, 2000.
[3] D.F. Moore, The friction and lubrication of elastomers, Pergamon, 1972.
[4] P. Jayawickrama, B. Thomas, Correction of field skid measurements for seasonal variations in Texas, Transport. Res. Record: J. Transport. Res. Board 1639 (1998) 147–154.

[5] J.G. Rose, B.M. Gallaway, Water depth influence on pavement friction, J. Transport. Eng. 103 (4) (1977) 491–506.
[6] J.C. Wambold, J.J. Henry, R.R. Hegmon, Skid resistance of wet-weather accident sites, The Tire Pavement Interface, ASTM Int. (1986) 47–60.
[7] J.C. Nicholls, I.G. Carswell, Effectiveness of edge drainage details for use with porous asphalt, TRL REPORT 376, 2001.
[8] T. Fwa, S. Tan, Y. Guwe, Laboratory evaluation of clogging potential of porous asphalt mixtures, Transport. Res. Rec. J. Transport. Res. Board 1681 (1999) 43–49.
[9] R.C. Dreher, W. Horne, Phenomena of pneumatic tire hydroplaning, 1963.
[10] S.K. Agrawal, J.J. Henry, Technique for evaluating hydroplaning potential of pavements, Transport. Res. Rec. J. Transport. Res. Board 633 (1977) 1–7.
[11] W. Gengenback, Experimental investigation of tires on wet tracks, ATZ 70 (1968) 310–316.
[12] W.B. Horne, T.J. Leland, Influence of tire tread pattern and runway surface condition on braking friction and rolling resistance of a modern aircraft tire, 1962.
[13] G. Maycock, Second paper: studies on the skidding resistance of passenger-car tyres on wet surfaces, proceedings of the institution of mechanical engineers: automobile division 180(1) (1965) 122-157.
[14] G. Staughton, T. Williams, Tyre performance in wet surface conditions, 1970.
[15] A.R. Woodside, D. Woodward, Wet Skid Resistance, Highways, 4th., Elsevier, 2002, pp. 479–499.
[16] P. Colonna, N. Berloco, P. Intini, A. Perruccio, V. Ranieri, Evaluating skidding risk of a road layout for all types of vehicles, Transport. Res. Rec. J. Transport. Res. Board (2591) (2016) 94–102.
[17] R.A. Moyer, Skidding characteristics of road surfaces, Highway, Research Board Proceedings (1934).
[18] J.P. Trant Jr, NACA Research on Friction Measurements, The First International Skid Prevention Conference, Virginia Council of Highway Investigation and Research, Virginia, 1959, pp. 297–308.
[19] K. Holmes, Braking force/braking slip: Measurements over a range of conditions between 0 and 100 per cent slip, in: R.R. Laboratory (Ed.), 1970.
[20] W.B. Horne, G. Taylor, T.J. Yager, Review of causes and alleviation of low tire traction on wet runways, 1968.
[21] U.T. Joyner, Effects of pavement texture on wet-runway braking performance, 1968.
[22] T.J. Yager, W.A. Vogler, P. Baldasare, Evaluation of two transport aircraft and several ground test vehicle friction measurements obtained for various runway surface types and conditions. A summary of test results from joint FAA/NASA Runway Friction Program; 1990.
[23] R.F. Smiley, W.B. Horne, Mechanical properties of pneumatic tires with special reference to modern aircraft tires, 1958.
[24] D. Chen, S. Han, A. Ye, X. Ren, W. Wang, T. Wang, Prediction of tire–pavement friction based on asphalt mixture surface texture level and its distributions, Road Mater. Pavem. Design (2019) 1–20.
[25] B.M. Gallaway, R.E. Schiller, J.G. Rose, The effects of rainfall intensity, pavement cross slope, surface texture, and drainage length on pavement water depths, 1971.
[26] G.G. Balmer, Pavement texture: Its significance and development, Transportation Research Record: Journal of the Transportation Research Board, 666, 1978, 1–6.
[27] L. Poulikakos, R. Gubler, M. Partl, M. Pittet, L. Arnaud, A. Junod, A.-G. Dumont, E. Simond, Mechanical properties of porous asphalt, recommendations for standardization, 2006.
[28] J.T. Van Der Zwan, T. Goeman, H. Gruis, J. Swart, R. Oldenburger, Porous asphalt wearing courses in the Netherlands: State of the art review, Transportation Research Record: Journal of the Transportation Research Board, 1265, 1990.
[29] B. Gallaway, D. Ivey, G. Hayes, W. Ledbetter, R. Olson, D. Woods, R. Schiller Jr, Pavement and geometric design criteria for minimizing hydroplaning, 1979.
[30] R.A. Moyer, A Review of the Variables Affecting Pavement Slipperiness, The First International Skid Prevention Conference, Virginia, 1958, pp. 411–433.
[31] B.G. Page, New and Innovative Methods and Materials for Pavement Skid Resistance, 1977.
[32] R. McDaniel, W.D. Thornton, J.G. Dominguez, Field evaluation of porous asphalt pavement, Purdue University, Schools of Civil and Mechanical Engineering, 2004.
[33] A. Browne, H. Cheng, A. Kistler, Dynamic hydroplaning of pneumatic tires, Wear 20 (1) (1972) 1–28.
[34] H. Grogger, M. Weiss, Calculation of the three-dimensional free surface flow around an automobile tire, Tire Sci. Technol. 24 (1) (1996) 39–49.
[35] C. Martin, Hydroplaning of Tire Hydroplaning Final Report, Project B-608, Georgia Institute of Technology, 1966.
[36] S. Tsakonas, C. Henry, W. Jacobs, Hydrodynamics of aircraft tire hydroplanning, 1968.
[37] J. Cho, H. Lee, J. Sohn, G. Kim, J. Woo, Numerical investigation of hydroplaning characteristics of three-dimensional patterned tire, Eur. J. Mechan.-A/Solids 25 (6) (2006) 914–926.
[38] G.P. Ong, T. Fwa, Transverse pavement grooving against hydroplaning. I: Simulation model, J. Transport. Eng. 132 (6) (2006) 441–448.
[39] T. Fwa, G.P. Ong, Transverse pavement grooving against hydroplaning II: Design, J. Transport. Eng. 132 (6) (2006) 449–457.
[40] L. Zhang, G.P. Ong, T.F. Fwa, Numerical study on the influence of aggregate size on skid resistance performance of porous pavements, Asian Transport Stud. 3 (3) (2015) 284–297.
[41] K. Anupam, Numerical Simulation Of Vehicle Hydroplaning And Skid Resistance On Grooved Pavement, 2011.
[42] S. Srirangam, K. Anupam, A. Scarpas, C. Kasbergen, M. Kane, Safety aspects of wet asphalt pavement surfaces through field and numerical modeling investigations, Transport. Res. Rec. J. Transport. Res. Board 2446 (2014) 37–51.
[43] K. Anupam S. Santosh Kumar C. Kasbergen A. Scarpas M. Kane Finite element framework for the computation of runway friction of aircraft tires Transport. Res. Rec. J. Transport. Res. Board 2641 2017 126 138
[44] R.J. Charbeneau, M.E. Barrett, Drainage hydraulics of permeable friction courses, Water Resour. Res. 44 (4) (2008).
[45] V. Ranieri, G. Ying, J. Sansalone, Drainage modeling of roadway systems with porous friction courses, J. Transport. Eng. 138 (4) (2011) 395–405.
[46] L. Zhang, G.P. Ong, T.F. Fwa, Developing an analysis framework to quantify and compare skid resistance performance on porous and nonporous pavements, Transport. Res. Record 2369 (1) (2013) 77–86.
[47] S.K. Srirangam, K. Anupam, A. Scarpas, A. Kösters, Influence of temperature on tire-pavement friction-1: laboratory tests and finite element modeling, Transportation Research Board 92nd Annual Meeting, Washington, D.C., 2013.
[48] T.R. Board, E. National Academies of Sciences, Medicine, Guide for Pavement Friction, The National Academies Press, Washington, DC, 2009.
[49] A. Zegard, F. Helmand, T. Tang, K. Anupam, A. Scarpas, Rheological Properties of Tire Rubber Using Dynamic Shear Rheometer For Fem Tire-Pavement Interaction Studies, Eighth International Conference on Maintenance Rehabilitation of Pavements, Singapore, 2016.
[50] W.L. Allen, Subsurface drainage of pavement structures: Current Corps of Engineers and industry practice, Cold Regions Research and Engineering Lab Hanover NH, 1991.
[51] N. Ross, K. Russam, The depth of rain water on road surfaces, 1968.
[52] B.M. Gallaway, J.G. Rose, Macro-texture, friction, cross slope and wheel track depression measurements on 41 typical texas highway pavements, Texas Transportation Institute, Texas A & M University, 1970.